Turkish Journal of Electrical Engineering & Computer Sciences

http://journals.tubitak.gov.tr/elektrik/

Research Article

Turk J Elec Eng & Comp Sci
(2021) 29: 1495 – 1508

doi:10.3906/elk-1907-28

Model-based control for second-order piezo actuator system with hysteresis in time-delay environment

Saikat Kumar SHOME[1,2,*], **Sandip JANA**[1,2], **Arpita MUKHERJEE**[2], **Partha BHATTACHARJEE**[2]

[1]Academy of Scientific and Innovative Research, CSIR CMERI Campus, Durgapm, India

[2]CSIR Central Mechanical Engineering Research Institute, Ministry of Science and Technology, Durgapur, India

Received: 04.07.2019 • **Accepted/Published Online:** 01.10.2019 • **Final Version:** 31.05.2021

Abstract: Piezo actuated systems are promising solutions for precision positioning applications. In this paper, a piezoelectric actuator is modeled as a second-order system using the Dahl hysteresis model and the system parameters have been identified from experimental data. The modified internal model control (M-IMC) approach is presented, which not only improves control performance but also reduces associated controller hardware resources. System dead time is approximated using first-order Padé expansion and the proposed Smith predictor-based M-IMC for piezoelectric actuators is seen to offer satisfactory stable control response even for plants with large dead time. The control performance of the M-IMC has been examined for the piezo actuator system against different set point tracking inputs in the presence of a wide range of external disturbances such as plant parameter mismatch, white noise perturbation, and time delay. Simulation results depict the efficacy and versatility of M-IMC in terms of decreased overshoot and settling time compared to traditional IMC and PID designs.

Key words: Piezoelectric, internal model control, disturbance, hysteresis, nonlinearity, Dahl model

1. Introduction

Piezoelectric actuators (PZAs) are gaining wide acceptance, especially in the area of micro-nano positioning applications. In the past decade, these manipulators became an active area of global research, being an inevitable component of a wide array of mechanisms used in micro-nano factories. A few pertinent applications in this domain range from atomic force microscopes (AFMs) to desktop reconfigurable nano-factories, IC chip assembly lines, and even niche biological cell operators [1,2]. Advantages like enhanced blocking force, fast response characteristics, and capacity to attain subnanometric positioning accuracy makes PZAs flagship linear actuators for several industrial applications. However, PZA materials are inherently characterized by some nonlinear phenomena, primarily hysteresis, which limits the positional accuracy [3]. The first step in achieving a proper closed-loop control response is a suitable mathematical model encapsulating the physical system behavior. Several studies have been carried out for modeling nonlinear hysteresis of PZA like the Preisach model, Maxwell model, Duhem model, Prandtl–Ishkii model, Bouc Wen model, and Dahl model [4–8]. In this paper, the Dahl model has been used to encapsulate hysteresis of the piezo actuator as it has a relatively simple system model representation.

In the modern world, IMC controllers are popularly used in numerous process control industries as they facilitate accurate set point tracking of the process, especially in the presence of disturbances. Asymptotic tracking of

*Correspondence: saikatkshome@cmeri.res.in

prescribed trajectories and/or asymptotic rejection of disturbances of a system is a crucial problem in control theory. There are three different avenues to address these problems: a) tracking via dynamic inversion, b) adaptive tracking, and c) tracking through system internal models. Tracking by dynamic inversion comprises figuring out an exact initial system state and a precise control input with the objective that the system is accordingly set up to initial conditions and run and the reference signal is exactly tracked by the output [9]. This calls for "perfect knowledge" of the complete trajectory that is to be tracked along with "perfect knowledge" of the plant model that is to be controlled. This approach is not preferable for plants with large uncertainties for either parameters or the reference signal. Dynamic inversion plays a primary role in adaptive tracking where the control input parameters are tuned so as to achieve asymptotic convergence to zero tracking error [10].
This methodology can tackle the problem of parameter uncertainties with the restriction of a priori knowledge of the complete trajectory that is to be tracked to develop the adaptive strategy and hence not justified in cases where tracking trajectories are unknown. A reference trajectory with a very slow varying nature may be considered as a stabilizing issue with a gradual variation of unknown parameters but mostly leading to a very conservative solution. On the contrary, simultaneous handling of uncertainties of plant parameters as well as the trajectory that is to be tracked can be dealt with by internal model-based control. The principle of internal model control (IMC) states that if the trajectory to be tracked belongs to the set of all trajectories generated by some fixed dynamical system, a controller that incorporates an internal model of such a system is able to secure asymptotic decay to zero tracking error for every possible trajectory in this set and is also robust with respect to parameter uncertainties [11]. This offers a huge advantage compared to the other two approaches discussed earlier, where instead of presuming that a trajectory belongs to a class of trajectories set up by an exogenous system, one is required to know complete information of the trajectories' past, present, and future time history. Due to this flexibility, the internal model-based approach is the best suited for dealing with scenarios that involve rejecting unknown disturbances as well as tracking unknown references [12–14].
The contribution of this research is that it investigates the performance of a traditional IMC structure in piezoelectric actuation and examines its performance. A relatively less hardware-intensive solution in the form of modified IMC is presented for delay-free PZA systems, which, however, does not perform well for PZA processes with dead time. The proposed Smith predictor-based modified IMC framework confirms the satisfactory performance of the PZA system with dead time along with considerable robustness to disturbances.

2. Modified internal model control (M-IMC) for delay-free piezoelectric actuation system

Realization of an IMC structure centers around getting the exact model of the PZA plant and then using it as a reference model in a parallel loop of the PZA model. This procedure involves repetitive resource utilization, once for the model and then for the controller. M-IMC introduces some changes in the IMC structure to reduce the amount of hardware components for the controller. In spite of IMC being an easily implementable controller, PID control still remains the most commonly used industrial control. The presented design eliminates the additional parallel reference model along with the advantage of proposing a PID equivalent of the IMC with reduced controller tuning parameters.

2.1. Design approach

The following figures elaborate the transformation of classical IMC through block diagram manipulation. Figure 1 represents the typical IMC structure where $G_{PZA}(s)$ represents the actual process, $\tilde{G}_{PZA}(s)$ stands for the mathematical model (transfer function) of the process, $G_{INV}(s)$ is the transfer function of the classical IMC

controller, and $d(s)$ is the disturbance. Figure 2 shows the modified IMC control structure of the piezoelectric actuator system where the plant model has been shifted in the inner feedback loop. It is clear in Figure 2 that the inner feedback loop has R(s)–Y(s) as its input, which is the error term used by a standard feedback controller. Figure 3 shows that the modified IMC structure can be reorganized in the form of a feedback control loop, which is useful as it can be represented by an equivalent PID topology, which is widely used in common industrial applications. The PID tuning parameters have been derived from the modified IMC structure shown in Figure 4. The modified topology also has the advantage of reduced hardware resources as it brings about a single tunable control block in contrast to traditional IMC, which has two control blocks: the inverse controller and the process model.

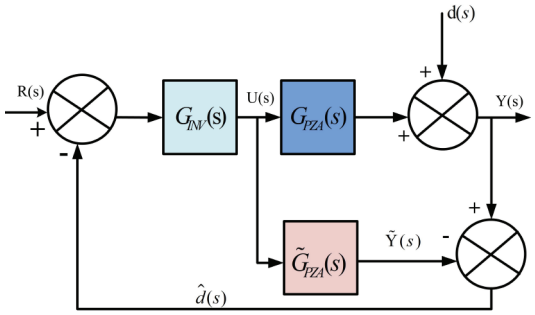

Figure 1. Conventional IMC structure for piezoelectric actuator system.

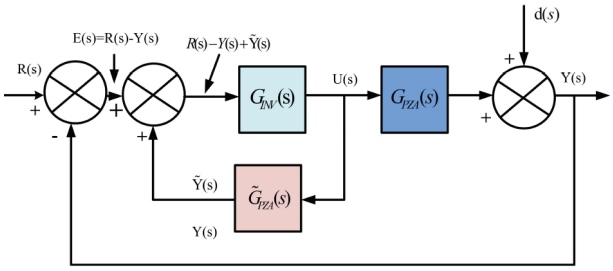

Figure 2. Modified IMC structure for piezoelectric actuator system.

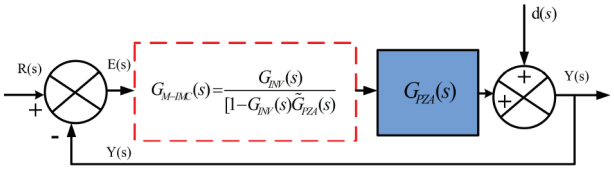

Figure 3. Simplified structure of modified IMC.

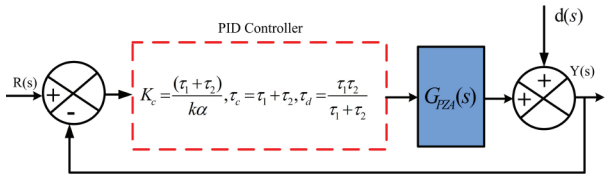

Figure 4. PID equivalent control structure of modified IMC.

A low-pass filter is augmented in series with the plant to make the system proper. This robust compensating filter plays an important role in the PZA system by handling different plant uncertainties in the system design so that the resultant controller can achieve the desired design objectives of robustness in performance and stability. The final form of the IMC controller with the augmented filter function is

$$G_{INV}(s) = \tilde{G}_{PZA}^{-1}(s) \cdot G_f(s), \tag{1}$$

where $G_f(s) = \frac{1}{(\alpha s+1)^n}$, n is the filter order, and α, the filter time-constant, is taken as 2. With the incorporation of the filter, the final form of the closed-loop transfer function that characterizes the system becomes

$$\tilde{G}_{PZA}(s) = \frac{k}{(\tau_1 s + 1)(\tau_2 s + 1)}. \tag{2}$$

The M-IMC controller transfer function is formulated according to the block schematic shown in Figure 4 as

$$G_{INV}(s) = \tilde{G}_{INV}(s) f(s) = \tilde{G}_{PZA}^{-1}(s) G_f(s). \tag{3}$$

The PZA plant can be conceptualized in invertible and noninvertible components as

$$\tilde{G}_{PZA}(s) = \tilde{G}_{PZA^+}(s) \cdot \tilde{G}_{PZA^-}(s). \tag{4}$$

$\tilde{G}_{PZA^+}(s)$ contains all nonminimum phase components and has been neglected. The process model can thus be represented as $\tilde{G}_{PZA}(s) = \tilde{G}_{PZA^-}(s)$. Therefore,

$$G_{INV}(s) = \tilde{G}^{-1}_{PZA^-}(s)G_f(s) = \frac{(\tau_1 s+1)(\tau_2 s+1)}{k}\frac{1}{\alpha s+1}, \tag{5}$$

where $G_f(s)$ is a filter in series with $\tilde{G}^{-1}_{PZA}(s)$ and the equation of the equivalent standard closed-loop controller is now

$$G_{M-IMC}(s) = \frac{G_{INV}(s)}{1-\tilde{G}_{PZA}(s)G_{INV}(s)} = \frac{\frac{(\tau_1 s+1)(\tau_2 s+1)}{k(\alpha s+1)}}{1-\frac{k\cdot(\tau_1 s+1)(\tau_2 s+1)}{(\tau_1 s+1)(\tau_2 s+1)k(\alpha s+1)}} = \frac{\tau_1\tau_2 s^2+(\tau_1+\tau_2)s+1}{k\alpha s}. \tag{6}$$

However, the transfer function of a standard PID controller is

$$g_c(s) = k_c[\frac{\tau_c\tau_d s^2+\tau_c s+1}{\tau_c s}]. \tag{7}$$

Equation 7 is multiplied by $\frac{\tau_1+\tau_2}{\tau_1+\tau_2}$ and rearranged to make it in the form of Equation 8 to find an equivalent to the PID structure. Thus,

$$G_{M-IMC}(s) = (\frac{\tau_1+\tau_2}{ka})\cdot\frac{\tau_1\tau_2 s^2+(\tau_1+\tau_2)s+1}{(\tau_1+\tau_2)s}. \tag{8}$$

Equating terms from Equation 7 and Equation 8 leads to $k_c = \frac{(\tau_1+\tau_2)}{ka}, \tau_c = (\tau_1+\tau_2), \tau_d = \frac{\tau_1\tau_2}{\tau_1+\tau_2}$. In this research, the piezo actuator transfer function has been found using the procedure described in Section 4, Equation 31, and is as follows:

$$G_{PZA}(s) = \tilde{G}_{PZA}(s) = \frac{0.0336}{0.1828s^2+190.154s+119206.85} = \frac{2.8186\times10^{-7}}{1.5334\times10^{-6}s^2+1.5951\times10^{-3}s+1}. \tag{9}$$

From Equation 2, we get

$$\tilde{G}_{PZA}(s) = \frac{k}{(\tau_1 s+1)(\tau_2 s+1)} = \frac{k}{\tau_1\tau_2 s^2+(\tau_1+\tau_2)s+1}. \tag{10}$$

The plant parameters have been identified comparing (9) and (10), which are then used in Equation 6 to represent the controller transfer function. Thus, the $G_{M-IMC}(s)$ controller can be represented as $\frac{4.3389\times10^{-3}s^2+4.5134s+2829.59}{1.5951\times10^{-3}s}$.

3. Modified internal model control for piezoelectric actuation system with time delay

A practical dynamical system does exhibit some time lag between the change of input and representation of the same in its output. There are different causes behind this time lag. In PZA systems, time delay may occur in the state of the system sensor measurements and transmission of the measurement of the system as seen by ΔT in Figure 5.

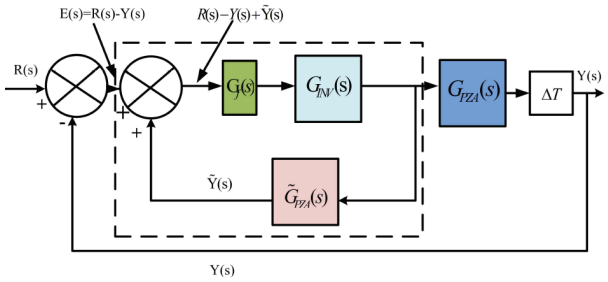

Figure 5. Modified IMC structure for piezoelectric actuator with time-delay system.

For a mathematical representation, this total phenomenon is aggregated and referred to as dead time or commonly as time delay. If the practical PZA system is modeled with time delay in the form of a time-invariant nonlinear system, the system transfer function becomes less rational due to the presence of this delay function. However, most of the methods used for analyzing and synthesizing control systems are for rational transfer functions. To use these methodologies for a dynamical PZA system, the time delay needs to be approximated through some rational function, mostly using Taylor series expansion of the exponential function or Padé approximation. In this research, Padé approximation is preferred as Taylor series expansion meets the weak conditions of physical realizability besides introducing unstable zeros in the system:

$$\tilde{G}_{PZA}(s) = \frac{ke^{-\Delta Ts}}{(\tau_1 s+1)(\tau_2 s+1)}. \tag{11}$$

First–order Padé approximation is used for dead time, yielding

$$e^{-\Delta Ts} = \frac{(-0.5\Delta Ts+1)}{(0.5\Delta Ts+1)}. \tag{12}$$

Hence, the PZA system is

$$\tilde{G}_{PZA}(s) = \frac{ke^{-\Delta Ts}}{(\tau_1 s+1)(\tau_2 s+1)} = \frac{k(-0.5\Delta Ts+1)}{(0.5\Delta Ts+1)(\tau_1 s+1)(\tau_2 s+1)}. \tag{13}$$

The system is then factorized into invertible and noninvertible components, with the invertible component being

$$\tilde{G}_{PZA^-}(s) = \frac{k}{(0.5\Delta Ts+1)(\tau_1 s+1)(\tau_2 s+1)}, \tag{14}$$

and $G_{PZA^+}(s) = (-0.5\Delta Ts+1)$ being the noninvertible term with RHP zero and nonminimum phase. Hence, the idealized controller $\tilde{G}_{INV}(s)$ is

$$\tilde{G}_{INV}(s) = \frac{(0.5\Delta Ts+1)(\tau_1 s+1)(\tau_2 s+1)}{k}. \tag{15}$$

The proposed controller is now augmented with a low-pass filter to make the controller proper, resulting in

$$G_{INV}(s) = \tilde{G}_{INV}(s)G_f(s) = \tilde{G}_{PZA^-}(s)G_f(s) = [\frac{(0.5\Delta Ts+1)(\tau_1 s+1)(\tau_2 s+1)}{k}](\frac{1}{\alpha s+1}). \tag{16}$$

The equivalent closed-loop M-IMC transfer function is obtained as from Eq. (4), Eq. (5), and Eq. (6):

$$G_{M-IMC}(s) = \frac{G_{INV}(s)}{1-\tilde{G}_{PZA}(s)G_{INV}(s)} = \frac{\tilde{G}_{INV}(s)G_f(s)}{1-\tilde{G}_{PZA}(s)\tilde{G}_{INV}(s)G_f(s)} = \frac{\tilde{G}_{INV}(s)G_f(s)}{1-\tilde{G}_{PZA^-}(s)\tilde{G}_{PZA^+}(s)\tilde{G}^{-1}_{PZA^-}(s)G_f(s)}, \quad (17)$$

$$G_{M-IMC}(s) = \frac{\tilde{G}_{INV}(s)G_f(s)}{1-\tilde{G}_{PZA^+}(s)G_f(s)} = \frac{[\frac{(0.5\Delta Ts+1)(\tau_1 s+1)(\tau_2 s+1)}{k}](\frac{1}{\alpha s+1})}{1-(-0.5\Delta Ts+1)(\frac{1}{\alpha s+1})}, \quad (18)$$

which leads to

$$G_{M-IMC}(s) = (\frac{1}{k})\frac{(0.5\Delta Ts+1)(\tau_1 s+1)(\tau_2 s+1)}{(\alpha+0.5\Delta T)s}. \quad (19)$$

3.1. Role of Smith predictor

Ideally, the time-delay affects the system response by shifting with the value of the time delay besides introducing a higher overshoot and a larger settling time. If the introduced time delay is large enough, the system response will be unbounded, leading to instability. Thus, traditional controllers cannot deal with systems with large time delay, leading to a well-recognized problem in control processes with an unsatisfactory performance. Smith predictor control topology helps overcome this drawback and facilitates larger gains. The PZA system can be conceptually split into a system of delay-free dynamics and a pure time-lag component, as shown in Figure 6a. A measurable variable would enable it to be connected to the controller, as in Figure 6b, which would shift the time delay out of the control loop. The closed-loop transfer function derived from the block diagram and Smith predictor control scheme [15] is given in Figure 6c:

$$\frac{Y(s)}{R(s)} = \frac{G_{INV}(s)G_{PZA}(s)\Delta T}{1+G_{INV}(s)\tilde{G}_{PZA}(s)-G_{INV}(s)\tilde{G}_{PZA}(s)\tilde{\Delta}T+G_{INV}(s)G_{PZA}(s)\Delta T}. \quad (20)$$

When the PZA model matches the PZA plant, the transfer function reduces to $G_{PZA}(s) = \tilde{G}_{PZA}(s)$,

$$\frac{Y(s)}{R(s)} = \frac{G_{INV}(s)G_{PZA}(s)\Delta T}{1+G_{INV}(s)\tilde{G}_{PZA}(s)}. \quad (21)$$

4. System modeling and identification

Dynamical modeling of the piezoelectric system has been expressed in the form of a second-order mass-spring-damper system with the nonlinear hysteretic effect being modeled using the Dahl hysteresis model [16,17], represented by the following equation:

$$M\ddot{x} + D\dot{x} + Kx = Tu - F_h, \quad (22)$$

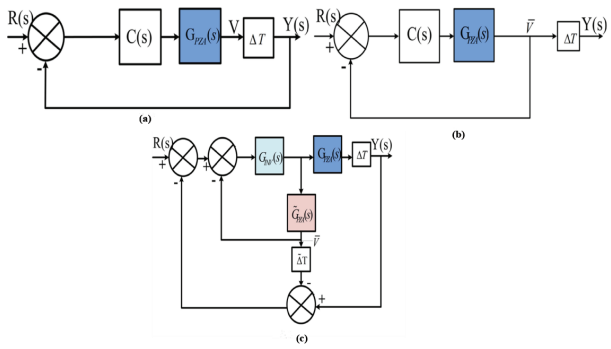

Figure 6. (a) Conventional time-delay system with feedback from Y, (b) conventional time-delay system with feedback from V, (c) IMC-based Smith predictor control scheme for piezoelectric actuator system.

where M, D, K, T, u, and F_h represent the system mass, damping coefficient, stiffness, piezoelectric coefficient, input voltage, and hysteresis effect in terms of force, respectively. The above hysteresis force can be represented with state vector V in state space form as

$$\dot{V} = (A_h\dot{x})V + (B_h u_p)\dot{x}, F_h = C_h V, \tag{23}$$

where the intermediate state vector $V = \begin{bmatrix} p_1 & p_2 \end{bmatrix}^T$, x denotes x-axis displacement, and u_p is taken as a constant of 30, and the matrices are

$$A_h = \begin{bmatrix} 0 & 1 \\ -a_2 & -sgn(\dot{x})a_1 \end{bmatrix}, B_h = \begin{bmatrix} 0 \\ 1 \end{bmatrix}, C_h = \begin{bmatrix} b_1 & sgn(\dot{x})b_0 \end{bmatrix}. \tag{24}$$

Thus, using the above Dahl model formulation, we have the following equations, which mathematically represent the nonlinear force and involve the hysteretic parameters:

$$\dot{p_1} = p_2\dot{x}, \dot{p_2} = -p_1 a_2\dot{x} - p_2 a_1 sgn(\dot{x})\dot{x} + u_p\dot{x}, F_h = p_1 b_1 + b_0 p_2 sgn(\dot{x}). \tag{25}$$

The hysteresis parameters a_1, a_2, b_0, and b_1 of the above equations can be experimentally determined from the following equations:

$$a_1 = \frac{2}{t_1 - t_2} \cdot \ln\frac{H_1 - H_s}{H_2 - H_s}, a_2 = \frac{4\pi^2}{(t_1 - t_2)^2} + \frac{a_1^2}{4}, b_1 = G_{dc}a_2, b_0 = S_0, \tag{26}$$

where $t_2 - t_1$ is the time period of the PZA damped oscillations in the time domain open-loop step response of the piezo actuator, as seen in Figure 7. H_1 and H_2 represent the height of the overshoot of the first and second peaks, respectively, and H_s is the steady state response, G_{dc} represents the dc gain, and S_0 is the initial slope of the response. For the below time domain step response, the DC gain, G_{dc}, is calculated as the ratio of H_s to the input step voltage, i.e. (21.1/75), and initial slope $S_0 = 0$.

Thus, we have

$$a_1 = \frac{2}{(0.021 - 0.0150)} \cdot \ln\frac{(28.6 - 21.1)}{(26.4 - 21.1)} = 115.732, \tag{27}$$

$$a_2 = \frac{4\pi^2}{(0.021 - 0.0150)^2} + \frac{115.732^2}{4} = 1098859.58, b_1 = 0.281 \cdot a_2, b_0 = 0. \tag{28}$$

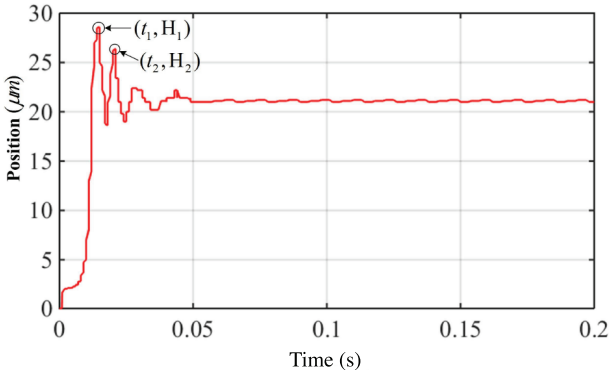

Figure 7. Open-loop time domain response of the piezoelectric actuator for 75 V input.

A state space representation of the entire piezoelectric system including the nonlinear hysteresis force can be represented as follows using state vector $X = [x, \dot{x}, p_1, p_2]^T$ and also as shown in Figures 8a and 8b:

$$\dot{X} = AX + Bu, Y = CX, \tag{29}$$

where the system, input, and output matrix are

$$A = \begin{bmatrix} 0 & 1 & 0 & 0 \\ -K/M & -D/M & -b_1/M & -(b_0/M)sgn(\dot{x}) \\ 0 & 0 & 0 & \dot{x} \\ 0 & u_p & -a_2\dot{x} & -a_1\dot{x}sgn(\dot{x}) \end{bmatrix}, B = \begin{bmatrix} 0 \\ T/M \\ 0 \\ 0 \end{bmatrix}, C = \begin{bmatrix} 1 & 0 & 0 & 0 \end{bmatrix}. \tag{30}$$

To identify the system parameters, input voltage at different frequencies (1 Hz, 10 Hz,) and different peak-peak amplitudes (10 V, 50 V) have experimentally been given to the piezoelectric actuator and outputs of the system have been used to identify the four dynamic parameters M, D, K, and T of the PZA transfer function model, as mentioned in Equation 31. The specifications of the actuator used in the study are mentioned in the Table. The experimental setup to determine the plant parameters of the piezoelectric actuator system is shown in Figure 9.

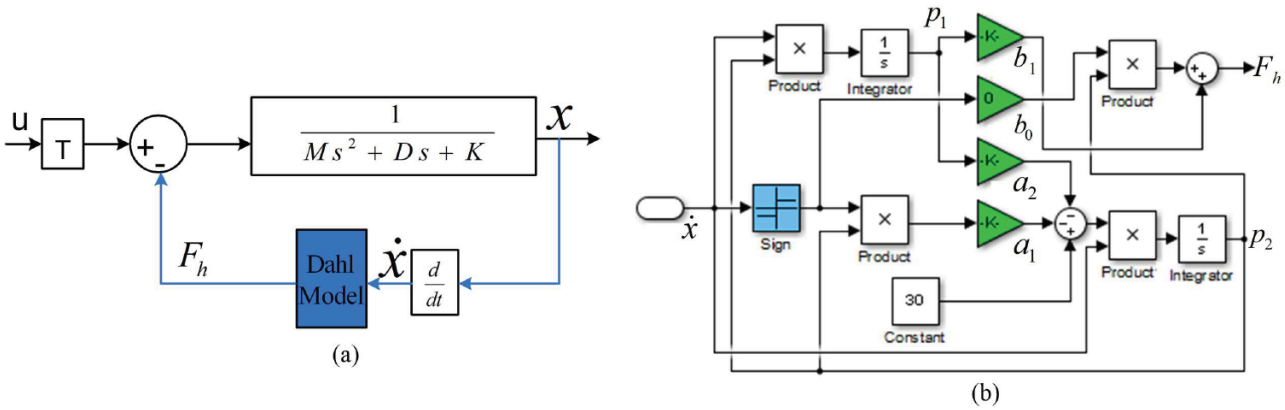

Figure 8. (a) Schematic block diagram of the entire piezoelectric system leading to output of x for input voltage u; (b)Dahl model for calculating the hysteresis force F_h.

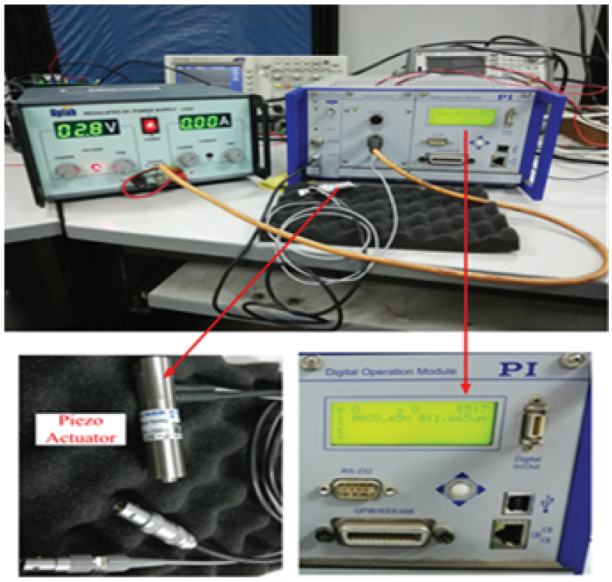

Figure 9. Experimental setup for determination of piezo actuator parameters.

$$TF = \frac{0.0336}{0.1828s^2 + 190.154s + 119206.85} = \frac{T}{Ms^2 + Ds + K}. \tag{31}$$

To observe the response of the PZA system, different external disturbances along with plant parameter variations were independently simulated and the performance of the controllers was observed.

Table 1. Table. Specifications of the piezo actuator.

Open-loop travel, at 0 to 100 V	30 μm
Closed-loop travel	30μm
Integrated feedback sensor	SGS
Resolution, closed-loop / open-loop	0.6 / 0.3 nm
Static large-signal stiffness	27$N/\mu m$
Electrical capacitance	3.0μF
Push force capacity	1000 N
Length	50 mm

5. Results and discussion

To verify the efficiency of the proposed controller in the presence of external perturbations, system disturbances, and parametric variations, different test cases have been used and are presented in the following sections. It is observed that for the proposed controller (M-IMC), tracking performance is better than that of the classical controller for piezo system dynamics. The system stability issue for large time-delay is successfully achieved by the Smith predictor-based controller.

5.1. Performance of M-IMC controller in presence of impulse disturbances at the PZA system output

The second-order PZA system is subjected to a unit impulse disturbance assuming no mismatch between process and model, as shown in Figure 10a. The response of the PZA system to an impulse disturbance (of width 20 starting from t = 20 s) is shown in Figure 10b.

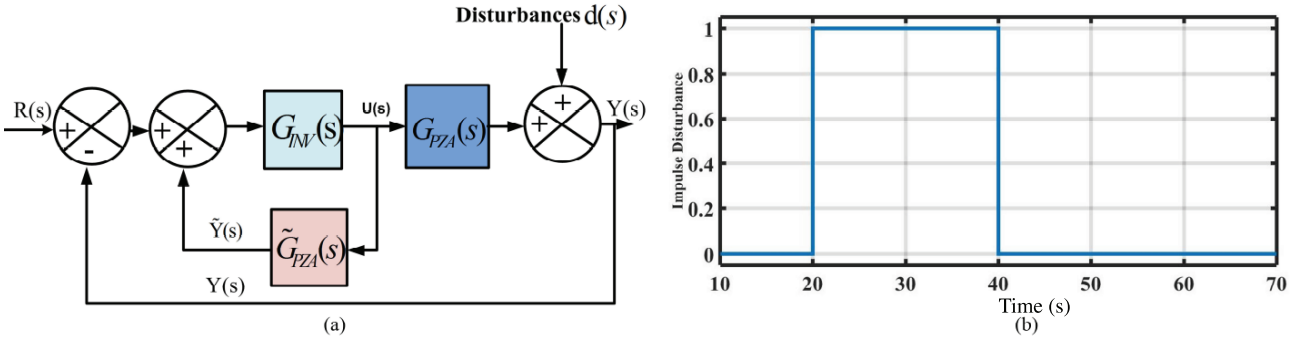

Figure 10. (a) M-IMC control structures with disturbances (impulse, band white noise). (b) Impulse disturbance of width 20 applied to the PZA system.

Though the input is provided to achieve zero tracking, it is seen that the response shifts to an amplitude of one due to the onset of the disturbance at the 20th second and the system gradually eliminates this effect and returns to zero owing to controller action. As the disturbance becomes zero at the 40th second, the system behaves in a reverse manner due to the sudden absence of the impulse and again returns to its set-point of zero as shown in Figure 11. No overshoot is observed and the system gradually achieves near-zero steady state error. It is observed that the effect of impulse disturbance is better compensated with M-IMC control at a settling time of 28 s while conventional IMC settles at 31 s and conventional PID at 36 s.

5.2. Band white noise disturbance at the PZA plant output

In a practical scenario, the plant may be subjected to random disturbances, which are not readily identifiable. A stochastic disturbance model in the form of band white noise (noise power, sample time of 0.1 s) is used to simulate unknown disturbances. The output is seen to reduce the effect of external disturbances and return to its set point, which is zero, as shown in Figure 12. It is seen that M-IMC control results are better as it seems to have a quicker nullification of the band white noise with less time response as shown in Figure 12.

5.3. Plant parameter variation at the PZA plant output

Plant/model mismatch is very common and practically unavoidable, which appears due to reasons such as measuring error, uncertainty in plant parameters, or treating higher-order systems as lower-ordered.

Besides, the piezo actuator system is nonlinear in nature, which enhances the chance of mismatch. In the following section, the controller works for a plant model that suffers from 10% plant parameter variation as compared to the nominal model and its performance has been observed by applying impulse disturbance to a unit step input. From the results it is clear that M-IMC is able to handle the uncertainties due to plant parameter variation in a much better way with less settling time and regulate its output to track the set point of unity in comparison to conventional IMC as shown in Figure 13, which steadies at a slightly shifted value other than one.

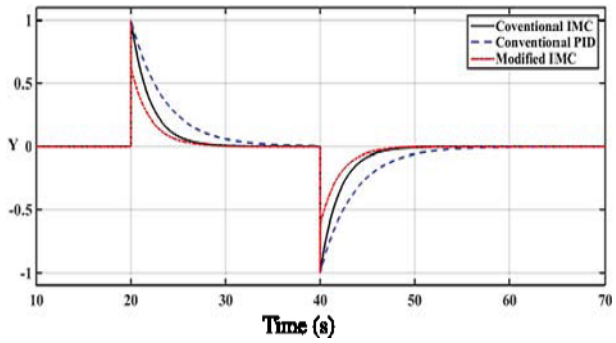

Figure 11. Response of conventional IMC, modified IMC, and conventional PID control schemes to impulse disturbance for PZA system.

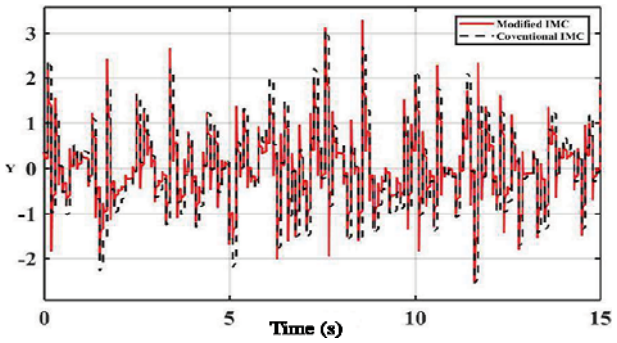

Figure 12. Effect of band white noise disturbance of conventional IMC and modified IMC for the PZA system.

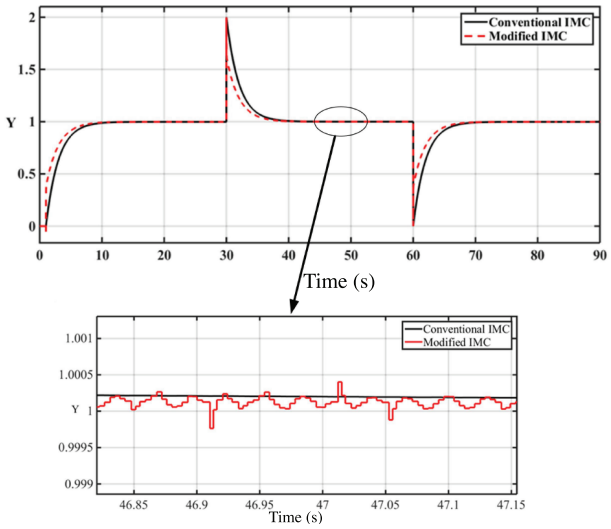

Figure 13. Step responses of modified IMC and conventional IMC with impulse disturbance due to 10% plant parameters variation.

5.4. PZA system stability issues in presence of large time-delay disturbance

Response of the PZA system in the presence of large time delay (5 s) and impulse disturbance is studied in this section. M-IMC with Smith predictor produces a stable output as shown in Figure 14a with an overshoot of 13% and settling time of 36.5 s and a suitable compensation of the impulse disturbance. System response changes considerably upon increasing the delay with the output gradually getting unbounded, and the system turns unstable with conventional IMC (Figure 14b).

5.5. Role of Smith predictor-based controller in compensating delay disturbance

Smith predictor-based design is useful to compensate the time lags occurring in physical systems, treating it as a delay-free process. The Smith predictor-based IMC controller is compared with normal IMC for a system with time delays of 2 s. The step response of a Smith predictor-based IMC is seen in Figure 15 to be better with a very shorter settling time of 11 s as compared to 16 s for without Smith predictor although with a slight overshoot.

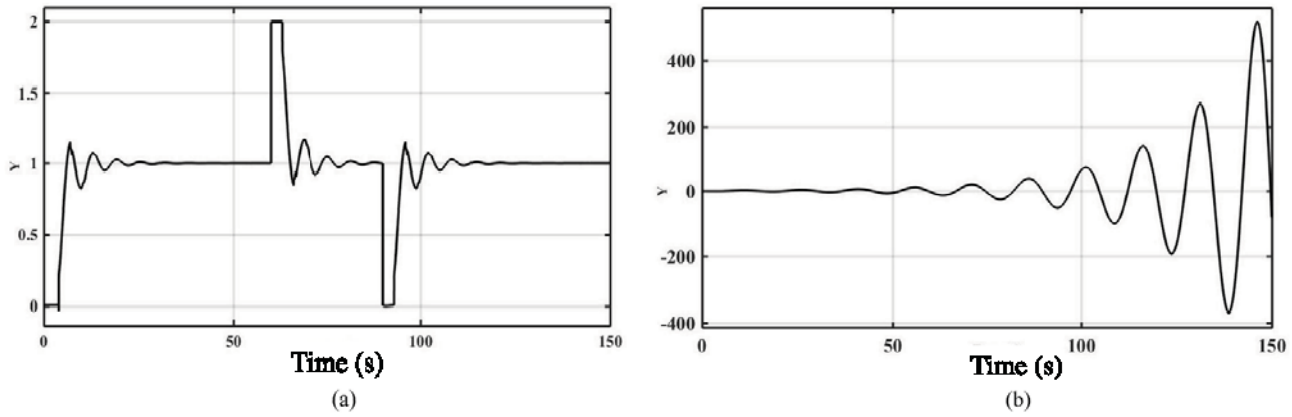

Figure 14. (a) Stability response of modified IMC with Smith predictor scheme in the presence of large time-delay disturbance $\Delta T = 5s$ and impulse disturbances. (b) Unstable response of conventional IMC scheme in the presence of large time-delay disturbances $\Delta T = 5s$ and impulse disturbances.

5.6. System performance in presence of time delay and step disturbance

Accordingly, a time delay of 2 s is assumed in the PZA system along with a mismatch of 0.5 s. Conventional IMC is seen to have an uneven response with the effect of the perturbation seen to persist for a longer time duration. On the other hand, M-IMC compensates the effect of the step disturbance with a comparatively smoother response and smaller settling time of 8.5 s compared to 30 s as shown in Figure 16.

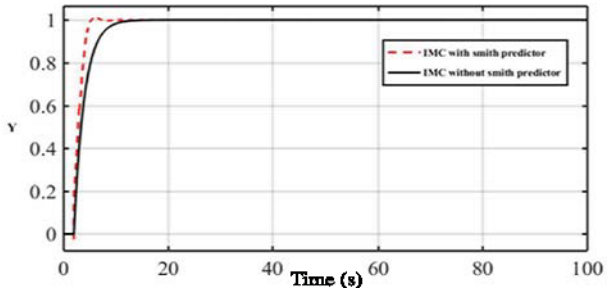

Figure 15. Step response of IMC-based Smith predictor and without Smith predictor for PZA.

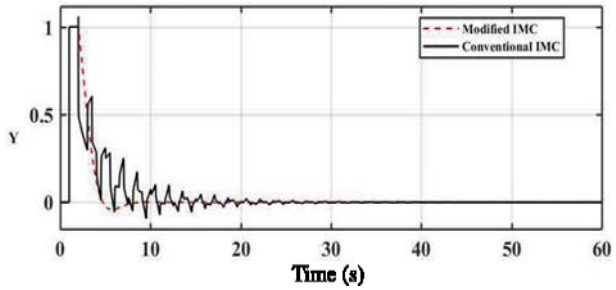

Figure 16. System performance response of conventional IMC and modified IMC with time delay for PZA system.

5.7. Step response of time-delayed PZA system with impulse disturbance

This subsection shows the performance of four different controllers towards the step response of the PZA system with a time delay of 1.5 s and an impulse disturbance. The conventional PID controller is seen to have the longest settling time of 84 s among the four after the impulse is given at t = 60 s, as seen in Figure 17. M-IMC performs better than conventional IMC with a settling time of 71 s and 75 s, respectively. The Smith predictor-based controller with M-IMC is seen to be the most efficient controller in terms of disturbance rejection and settles fastest at 69.5 s.

6. Conclusion

The present research focuses on the design of an efficient control structure targeting improved control performance of a piezo actuator in the presence of time delay. The M-IMC-based controller design with a low-pass filter has been presented for a piezo actuated micromanipulator. The system delay has been approximated using

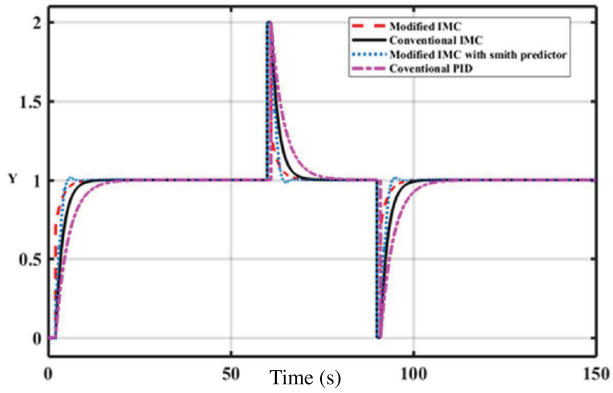

Figure 17. Step responses of different control schemes with impulse disturbances for time-delay PZA system.

first-order Padé approximation. The presented controller is seen to perform better for PZA systems with dead time compared to classical IMC; however, the system becomes unstable for higher values of time delay. The role of the Smith predictor-based M-IMC is also observed towards compensating the presence of large time delay and maintaining system stability with better control response. Results depict that the proposed M-IMC-based controller for PZA systems is better than both classical PID and IMC in terms of common control parameters.

7. Acknowledgment

The authors gratefully acknowledge the funding received from the Indo French Center for the Promotion of Advanced Research (IFCPAR/CEFIPRA) for carrying out this work.

References

[1] Binnig G, Rohrer H. Scanning tunneling microscopy. Helvetica Physica Acta 1983; 55: 726-735.

[2] Binnig G, Quate CF, Gerber C. Atomic force microscope. Physics Review Letters 1986; 56: 930-933.

[3] Devasia S, Eleftheriou E, Moheimani R. A survey of control issues in nanopositioning. IEEE Transactions on Control Systems Technology 2007; 15 (5): 205-213. doi: 10.1109/TCST.2007.903345

[4] Song G, Zhao J, Zhou X, de Abreu-García JA. Tracking control of a piezoceramic actuator with hysteresis compensation using inverse Preisach model. IEEE/ASME Transactions on Mechatronics 2005; 10 (2): 198-209. doi: 10.1109/TMECH.2005.844708

[5] Ge P, Jouaneh M. Modeling hysteresis in piezoceramic actuators. Precision Engineering; 1995; 17 (3): 211-221. doi: 10.1016/0141-6359(95)00002-U

[6] Weibel F, Michellod Y, Mullhaupt P, Gillet D. Real-time compensation of hysteresis in a piezoelectric-stack actuator tracking a stochastic reference. In: Proceedings of the American Control Conference; Seattle, WA, USA; 2008. pp. 2939-2944.

[7] Kuhnen K. Modeling identification and compensation of complex hysteretic non-linearities: a modified Prandtl–Ishlinskii approach. European Journal of Control 2003; 9 (4): 407-418. doi: 10.3166/ejc

[8] Shome SK, Prakash M, Pradhan S. Mukherjee A. On synergistic integration of adaptive dithering based internal model control for hysteresis compensation in piezoactuated nanopositioner. Mathematical Problems in Engineering 2015; 2015: 1-19. doi: 10.1155/2015/365141

[9] Hou G, Huang Y, Du H, Zhang J, Zheng X. Design of internal model controller based on ITAE index and its application in boiler combustion control system. In: 12th IEEE Conference on Industrial Electronics and Applications; Siem Reap, Cambodia; 2017. pp. 2078-2083.

[10] Liu T, Gao F. Enhanced IMC design of load disturbance rejection for integrating and unstable processes with slow dynamics. ISA Transactions 2011; 50 (2): 239-248. doi: 10.1016/j.isatra

[11] Xu Q, Li Y. Robust Process Control. Hoboken, NJ, USA: Prentice Hall, 1989.

[12] Naik K, Srikanth P, Negi P. IMC tuned PID governor controller for hydro power plant with water hammer effect. Procedia Technology 2012; 4 (2012): 845-853. doi: 10.1016/j.protcy

[13] Negi P. Frequency domain analysis of optimal tuned IMC-PID controller for continuous stirred tank reactor. International Journal of Electronics 2014; 2: 34-39.

[14] Shome SK, Jana S, Mukherjee A, Bhattacharjee P, Datta U. Improved internal model control based closed loop controller design for second order piezoelectric system with dead time. In: Proceedings of 2018 8th IEEE India International Conference on Power Electronics; Jaipur, India; 2018. pp. 1-6.

[15] Bahill A. A simple adaptive Smith-predictor for controlling time-delay systems. IEEE Control Systems Magazine 1983; 3 (2): 16-22. doi: 10.1109/MCS.1983.1104748

[16] Shome SK, Pradhan S, Mukherjee A, Datta U. Dither based precise position control of piezo actuated micro-nano manipulator. In: Proceedings of the 39th Annual Conference of the IEEE Industrial Electronics Society; Vienna, Austria; 2013. pp. 3486-3491.

[17] Xu Q, Li Y. Dahl model-based hysteresis compensation and precise positioning control of an XY parallel micromanipulator with piezoelectric actuation. Journal of Dynamic System, Measurement and Control 2010; 132 (4): 41011. doi: 10.1115/1.400171